RSC Advances

ROYAL SOCIETY OF CHEMISTRY

www.rsc.org/advances

Low Temperature Chlorobenzene Catalytic Oxidation over MnO_X/CNTs with the Assistance of Ozone

Dongdong Jin[1], Zhiyuan Ren[2], Zhaoxia Ma[1], Fu liu[1], Hangsheng Yang[1*]

[1] *State Key Laboratory of Silicon Materials, Department of Materials Science and Engineering, Zhejiang University, Zheda Road 38, Hangzhou 310027, China*

[2]*Foreign Economic Cooperation Office, Ministry of Environmental Protection,China, No 5 HouyingfangHutong, Xicheng District, Beijing 100035, China*

*To whom correspondence should be addressed. Tel/Fax: +86-571-87951404;

E-mail: hsyang@zju.edu.cn

Abstract: Carbon nanotubes supported manganese oxide (MnO_x/CNTs) were prepared by impregnation method and their catalytic oxidation performances of chlorobenzene (CB) with the assistance of ozone were investigated. Experimental results indicated a synergistic effect between MnO_x/CNTs catalyst and ozone promotion for CB destruction, which promoted CB oxidation at temperature between 80 °C and 280 °C. Especially at temperature below 120 °C, both CB conversion and CO_2 selectivity above 95 % were achieved with an apparent activation energy of 15.0 KJ/mol. Moreover, MnO_x/CNTs showed good stability and resistance to chlorine poisoning, which was demonstrated by a stable catalytic activity for a long-term CB catalytic oxidation up to 240 h.

Key words: MnO_x/CNTs; ozone; chlorobenzene; catalytic oxidation;

1. Introduction

Polychlorinated dibenzodioxins and polychlorinated dibenzofurans (PCDD/Fs, also defined as dioxins), which are mainly produced unintentionally in high temperature processes such as waste incineration and metallurgical industries, are a group of unintentionally persistent organic pollutants (UP-POPs) [Stockholm convention, http://chm.pops.int/TheConvention/ThePOPs/The12InitialPOPs/tabid/296/Default.aspx]. These compounds are very toxic, carcinogenic, and environmentally persistent. The emission of dioxins has been one of the most focused topics in global environmental problems. Stringent environmental regulations and standards are established to limit dioxins emission [1]. A series of techniques have been developed for dioxins removal including adsorption, thermal combustion, and catalytic oxidation [2]. Among them, catalytic oxidation is the most promising technology which can completely oxidize dioxins into CO_2, H_2O and HCl (or Cl_2) at relatively low temperatures. Catalytic oxidation can also be used to remove very dilute pollutants (<1 %) which cannot be thermally combusted without fuel addition efficiently. These distinct energy and economic efficiencies have attracted great attentions [3]. By the way, chlorobenzene (CB) is normally selected as model molecular in laboratory to optimize catalysts used for dioxins catalytic oxidation [4].

Normally, noble metals [5], perovskites [6] and transition metal oxides [7] are major candidates for catalyst optimization. Noble metals generally show high activity for the destruction of volatile organic compounds (VOCs) at relatively low temperatures [8],

however, they are not ideal catalysts due to high cost and severe deactivation from chlorine poisoning [9]. Perovskites are activated only at temperatures above 500 °C which lead to high energy consumption [10]. Therefore, many researches are focused on transition metal oxides (supported or unsupported), such as MnO_2, V_2O_5, Cr_2O_3 and so on [11-18]. Among them, MnO_x based catalyst is one of the most studied catalysts for CB catalytic oxidation, which exhibits excellent activity at temperature between 220 and 300 °C, and shows great resistance to chlorine poisoning [19]. However, the operation temperature is still high and there is a strong need to further reduce the catalytic oxidation temperature.

Ozone, as a strong oxidizer, can react with most organic compounds at low temperature (even at room temperature). Recently, several reports show that adding ozone into the catalytic oxidation process of VOCs can dramatically reduce the operation temperature and activation energy (E_a). For example, ozone can promote the catalytic oxidation of VOCs at temperatures below 200 °C [20, 21]. Even at room temperature, a benzene conversion of approximately 80 % is reported over MnO_x/Al_2O_3 catalyst with the assistance of ozone [22, 23]. But the low CO_2 selectivity is still a main barrier for its possible application to promote VOCs catalytic oxidation [22]. At the same time, carbon nanotubes (CNTs) [24], a novel nanomaterial, is reported to be an excellent VOCs adsorbent [25, 26], and the addition of CNTs into metal oxide catalysts promotes the CB oxidation evidently [27]. Previous studies indicated that the surface of CNTs could be modified by metal and metal oxide nanoparticles with good stability, according to which, it is expected that MeO_X/CNTs are also stable in the presence of

ozone [28]. We also find that ozone promoted CB catalytic oxidation at a wide temperature range between 100 °C and 300 °C over CuO/CNTs, and CNTs in the catalyst showed a good stability in the presence of ozone [29].

. In this study, the performance of CB catalytic oxidation over MnO_x/CNTs with the ozone assistance was studied, and our results indicated that with the assistance of ozone, CB could be completely degraded at temperature as low as 80 °C.

2. Experimental section

2.1 Catalyst preparation and characterization

MnO_x/CNTs composite was prepared by impregnation method. At first, 10.0 g Multi-walled carbon nanotubes (Shenzhen Nanoport Co. Ltd) were purified in 69 % HNO_3 at 60 °C for 3 h, followed by filtrated and washed with deionized water to a pH value of 7. Then, 350 mL aqueous solution of $Mn(CH_3COO)_2$ was used to impregnate the purified CNTs under vigorous stirring at 50 °C for 12 h. Finally, the suspension liquid was dried at 100 °C and then calcined at 450 °C for 2 h in N_2 so that MnO_x/CNTs with a theoretical MnO_x loading of 15.0 wt.% can be obtained.

The real Mn loading was measured to be 7.13 wt.% by X-ray energy dispersive spectroscopy (EDX; EDAX Genesis-4000) and the BET surface area of catalyst was calculated as 133.5 m^2/g by N_2-Physisorption (BET; Quantachrome Autosorb-1-C). X-ray powder diffraction (XRD; PANalytical X'Pert PRO) with Cu $K\alpha_1$ radiation (λ = 0.15406 nm), scanning electron microscopy (SEM; Hitachi S-4800), X-ray photoelectron spectroscopy (XPS; Thermo ESCALAB-250) were also used for the

characterization of fresh and used catalysts (after being used at 120 ℃ for 240 h under high O_3 concentration of 2300 ppm). The X-ray source was an Al Kα radiation, and all binding energies were referenced to the peak at 284.8 eV attributed to C1s.

. Moreover, H_2-temperature-programmed reduction (H_2-TPR) experiments were performed using 100 mg of each catalyst. The samples were pretreated under a N_2 gas flow at 200 ℃ for 1.5 h. TPR experiments were performed at a heating rate of 10 ℃/min under a mixed flow of 5 % H_2 in argon at a flow rate of 40 mL/min. The H_2-TPR data were recorded using an on-line gas chromatograph equipped with a thermal conductivity detector.

2.2 Catalytic activity characterization

2.5 g of catalyst was uniformly coated on 7 aluminum plates (4 cm×10 cm), which was then inserted into a fixed bed flow reactor for CB oxidation test, and the distance between two plates is approximately 3 mm, and the geometry of the reactor is shown in Supporting Information. The geometry of the SCR reactor has been shown in our previous study [30]. CB was carried by N_2 using a saturator maintained at 40 ℃, and a mixture of 20 % O_2 + 80 % N_2 was used as reactant gas to control a CB concentration of 30-500 ppm. Ozone was generated using 20 % O_2 + 80 % N_2 by an ozone generator, which could produce a maximum O_3 concentration of 4000 ppm under a gas flow of 1000 sccm. The reactant stream was preheated to 80 ℃ before entering into the reactor. A gas chromatograph (GC 9790) online apparatus equipped with flame ionization thermal conductivity detector (FITD) was used to measure CB (SE-54 column) and

CO_2 (porapakq-Q column) concentrations with an experimental error less than 5 %.

In this study, the catalytic activity was expressed herein in terms of CB conversion, CO_2 selectivity and CB complete conversion:

$$\text{CB conversion (\%)} = (CB_{inlet} - CB_{outlet}) \div CB_{inlet} \quad (1)$$

$$CO_2 \text{ selectivity (\%)} = CO_{2output} \div [6 \times (CB_{inlet} - CB_{outlet})] \quad (2)$$

$$\text{CB complete conversion (\%)} = CO_{2output} \div (6 \times CB_{inlet}) = \text{CB conversion} \times CO_2 \text{ selectivity} \quad (3)$$

3. Results and discussion

3.1 XRD and SEM analysis

The XRD patterns of fresh and used MnO_x/CNTs were shown in Fig. 1. Diffraction peaks corresponding to CNTs and MnO_x (MnO_2 and Mn_2O_3) [31] were detected, indicating that the structure of CNTs remained and different valence states of Mn species existed on CNTs. Typical SEM images with low, medium and high magnification in Fig. 2 showed the morphology of fresh (a, b, c) and used (d, e, f) catalysts (another low magnification SEM image of used catalyst is shown in Supporting Information). It could be observed that MnO_x was dispersed on the surface of multi-walled CNTs. Some aggregation of MnO_x particles could also be found, which reduced the BET surface area (S_{BET}) of catalyst to 133.5 m^2/g, while the S_{BET} of pristine CNTs was measured to be 270 m^2/g. Besides, there was no significant difference between fresh and used MnO_x/CNTs in XRD and SEM results, indicating the good stability of catalysts.

3.2 XPS analysis

In order to further investigate the catalysts, XPS spectra of fresh and used MnO_x/CNTs were collected and fitted by XPSPEAK 4.1 software. The XPS fully scanned spectra presented in Fig. 3 also showed the similar results between fresh and used catalysts. Moreover, signal of chlorine could hardly be detected in the used catalyst, indicating no Cl accumulation on the surface of the used catalyst, which suggested the great resistance to chlorine poisoning.

The XPS spectra of Mn 2p and O 1s were presented in Fig. 4, and the XPS analysis data were summarized in Table 1. Four peaks centered at 640.7, 642.0, 652.4, and 653.7 eV were observed in Mn 2p XPS spectrum (Fig. 4a), among which peaks centered at 640.7, 652.4 eV could be attributed to Mn^{3+} and peaks centered at 642.0, 653.7 eV could be attributed to Mn^{4+}. As can be seen in Table 1, the ratio of Mn^{4+}/Mn^{3+} of fresh catalyst (4.03) was higher than that of used catalyst (1.97), indicating that the surface Mn^{4+} species were reduced to Mn^{3+} species during the long-term reaction process even with O_3 assistance. Thus it can be inferred that Mn species in MnO_x/CNTs catalyst were involved in CB oxidation [32]. Fig. 4b showed the XPS spectra of O 1s for the fresh and used catalysts. In all spectra, O 1s spectra could be deconvoluted into three peaks at 529.7, 531.4 and 533.0 eV, corresponding to the lattice oxygen (O_{latt}, O^{2-}), adsorbed oxygen (O_{ads}, e.g., O radicals, O_2^-, O_2^{2-} or O^-), and adsorbed OH groups or molecular water (O_{sur}), respectively [33]. As calculated in Table 1, after being used for CB catalytic oxidation at 120 °C for 240 h under high O_3 concentration of 2300 ppm, the atomic concentration of O_{latt} decreased from 2.75 at.% to 1.85 at.%, which was in good agreement with reduction of the Mn^{4+}/Mn^{3+}ratio shown in Fig. 4a. In contrast, the

atomic concentrations of O_{ads} and O_{sur} increased from 4.17 at.% to 5.81 at.% and 1.24 at.% to 1.99 at.%, respectively, which were derived from O_3 decomposition. In fact, the increase of O_{ads} was suggested to be helpful for its catalytic activity [34, 35] and the existence of CNTs in catalyst was reported as an excellent CB adsorbent [25, 26, 36]. Therefore, O_{ads} species were ready to react with the adsorbed CB molecules thoroughly, thus promoting the catalytic oxidation of CB.

3.3 TPR analysis

To investigate the reducibility of the catalyst, H_2-TPR profiles were tested and shown in Fig. 5. For fresh catalyst, the H_2-TPR spectrum showed two peak centered at 360 and 500 °C. These two peaks could be ascribed to the two-step reduction of MnO_2. The first step corresponded to the reduction of MnO_2 to Mn_3O_4 and the second step represented the further reduction of Mn_3O_4 to MnO [37]. Moreover, the overlapped peak at 500 °C might also contain the reduction of Mn_2O_3 to Mn_3O_4 in the first step and further reduction to MnO [38]. Compared with fresh catalyst, the peak attributed to Mn^{4+} reduction in spectrum obtained from the used catalyst was weaker, which was in agreement with the XPS results shown in Fig. 4a.

3.4 Catalytic activity characterization

Figure 6 presented the CB oxidation efficiency over the MnO_x/CNTs. For reactions in the absence of O_3, the catalyst was almost inactive below 240 °C, which was consistent with the high-temperature reduction peak at 360 °C in the TPR profiles. The CB conversion was less than 20 % even at 240 °C and the CO_2 selectivity was also as

low as 30 % and 55 % at 80 °C and 240 °C, respectively. When O_3 was added, the CB removal efficiency increased remarkably. As was shown in Fig. 6a, the CB conversion reached 80 % and 95 % at 80 °C under O_3 concentration of 513 ppm and 2300 ppm, respectively. CO_2 selectivity also enhanced with O_3. Even at 80 °C, the CO_2 selectivity increased to 44 % under 50 ppm CB and 513 ppm O_3. Particularly under high O_3 concentration of 2300 ppm, a CO_2 selectivity of almost 100 % was achieved at 80 °C. Besides, with the increase of CB concentration, both CB conversion and CO_2 selectivity decreased due to the deficiency of O_3. At the same time, increasing the reaction temperature also induced the decrease of catalyst activity, and CO_2 selectivity reduced to 78 % at 240 °C even at high O_3 concentration of 2300ppm, which could be attributed to the quick combination of O radicals to O_2 [39]. By the way, in this study, no signal of CO was detected throughout our test, while some trace fragments of organic materials could be detected from gas chromatographer. However, at the present stage, the determination of these intermediate products from CB oxidation is still a challenge for us.

Since the concentration of VOCs in flue gases was usually very low, Fig. 7 showed dependence of CB complete conversion on O_3 concentration and temperature under low CB concentration of 50 ppm. For comparison, CB complete conversion obtained by O_3 only was also shown. The CB complete conversion of O_3 promoted catalysis was higher than the sum of CB complete conversion over catalyst only and O_3 only, indicating the synergistic effect of the catalyst and O_3 for CB destruction. Fig. 6 also showed that under high O_3 concentration of 2300 ppm, a CB complete conversion up

to 95 % could be achieved at 80 °C, suggesting the possibility to completely oxidize CB to CO_2 at very low temperature.

3.5 Kinetic study

Similar to our previous study [29], in this study, the CB oxidation could be considered to follow the Langmuir-Hinshelwood (L-H) mechanism. The reaction rate of CB oxidation can be expressed as equation (4) [40]:

$$-\mathrm{r} = \frac{kK_{CB}C_{CB}\sqrt{K_{O_3}C_{O_3}}}{\left(1+K_{CB}C_{CB}+\sqrt{K_{O_3}C_{O_3}}\right)^2} \quad (4)$$

Where r is the reaction rate (ppm/s), k is the rate constant, K_{CB} and K_{O3} are the equilibrium constants for CB and O_3 adsorptions, and C_{CB} and C_{O3} are the concentrations of the CB and O_3.

Considering that the concentrations of CB and O_3 are normally low (ppm), equation (4) can be further simplified to equation (5):

$$-\mathrm{r} = kK_{CB}C_{CB}\sqrt{K_{O_3}C_{O_3}} \quad (5)$$

From the dependence of k on the CB and O_3 concentrations presented in Fig. 8a, it was evident that the experimental data matched well with the modeled reaction route for CB catalytic oxidation. The apparent activation energy (Ea) was evaluated to be approximately 15.0 kJ/mol from Arrhenius plot between reaction temperatures and k shown in Fig. 8b, which was in good agreement with recent published results [29, 40]. In the absence of ozone, previous studies revealed that the Ea was 48 kJ/mol over manganese oxide for the CB catalytic oxidation [20], suggesting that the activation energy for the oxidation reaction was significantly reduced when O_3 instead of O_2 was

applied.

According to the above mentioned analyses, the O_3 promotion of CB oxidation over MnO_x/CNTs could be described as follows: MnO_x was highly dispersed on CNTs which could selectively adsorb both CB and O_3; O_3 decomposed on the catalyst surface which produced adsorbed oxygen radicals (O radicals or O_{ads}); oxygen radicals could efficiently react with adsorbed CB through L-H route. In order to completely oxidize CB into H_2O, CO_2, and HCl (or Cl_2), the strong CB adsorptivity of CNTs, which prolonged the residence time of CB on the catalysts surface thus prolonging the interaction time between CB and O_3 [36], should be essential, or else, the CO_2 selectivity would be low [22, 23]. Similar to O_3 promoted ethanol and ethane oxidation [41], catalytic decomposition of ozone was also closely associated with CB oxidation. In this study, highly dispersed MnO_x could promote O_3 decomposition below 120 °C [42], which generated large amounts of highly active oxygen species (O radicals and O_{ads}), and thus excellent performances of CB oxidation at low temperature could be achieved. However, with the increase of temperature, the side reaction of O radical combination to O_2 would increase, and the performances of CB catalytic oxidation with the assistance of ozone would be suppressed. Therefore, there is an optimal temperature, at which the surface concentration of oxygen radicals was maximized and the best performance of catalytic reaction was achieved.

Compared with our previous study for CB catalytic oxidation over CuO/CNTs [29], the temperature dependent of CB catalytic oxidation over these two catalysts are quite different. The optimal temperature for CB removal over MnO_x/CNTs was found to be

below 120 °C with the assistance of O_3. While CB oxidation over CuO/CNTs increased with temperature rising and got the optimal temperature at 240 °C. From literature, the O_3 decomposition was strongly dependent on the semi-conductive properties of metal oxide catalysts [39]. P-type oxides were found to be more active for O_3 decomposition than n-type ones, and MnO_x was reported to be the most active catalyst for O_3 decomposition. In contrast, CuO was an n-type oxide with the poorest activity [42, 43]. In the case of CB oxidation over MnO_x/CNTs, O_3 molecules decomposed fast even at low temperature, so the maximal oxygen radical concentration was achieved at relatively low temperature below 120 °C. While in the case of reaction over CuO/CNTs, O_3 decomposition was delayed and the maximal oxygen radicals' concentration was obtained above 240 °C. Therefore, it seemed that the optimal temperature of catalytic reaction with O_3 could be adjusted by modifying property of metal oxide catalysts.

4. Conclusion

In summary, we found that O_3 efficiently promoted CB catalytic oxidation over MnO_x/CNTs at only 80 °C and CB conversion and CO_2 selectivity above 95 % can be achieved. These phenomena could be attributed to the synergistic effect of O_3 decomposition and CB oxidation during catalytic reaction. Our findings can be extended to investigate the effect of p-type and n-type oxide on chlorobenzene catalytic oxidation with ozone and provide possible application of O_3 promotion for unintentionally persistent organic pollutants catalytic oxidation over semi-conduct metal oxides at low temperature.

Acknowledgements

This work was supported by the GEF project of Environmentally Sustainable Management of Medical Wastes in China, Global Environment Facility (Project No. GF/CPR/07/X02), the National Natural Foundation of Zhejiang Province, China (Grant No.Z4080070), and Zhejiang Province Environmental Protection Science Research Plan of China (2011B14).

References

1. R. Weber, T. Sakurai and H. Hagenmaier, *Appl. Catal. B-Environ.*, 1999, **20**, 249-256.
2. J. J. Spivey and J. B. Butt, *Catal. Today*, 1992, **11**, 465-500.
3. G. J. Hutchings, C. S. Heneghan, I. D. Hudson and S. H. Taylor, *Nature*, 1996, **384**, 341-343.
4. D. P. Debecker, F. Bertinchamps, N. Blangenois, P. Eloy and E. M. Gaigneaux, *Appl. Catal. B-Environ.*, 2007, **74**, 223-232.
5. L. Pinard, J. Mijoin, P. Magnoux and M. Guisnet, *J. Catal.*, 2003, **215**, 234-244.
6. R. Schneider, D. Kiessling and G. Wendt, *Appl. Catal. B-Environ.*, 2000, **28**, 187-195.
7. E. Kantzer, D. Döbber, D. Kießling and G. Wendt, *Scientific Bases for the Preparation of Heterogeneous Catalysts*, 2002, **143**, 489-497.
8. T. Maillet, C. Solleau, J. Barbier-Jr and D. Duprez, *Appl. Catal. B-Environ.*, 1997, **14**, 85-95.
9. B. Mendyka, A. Musialikpiotrowska and K. Syczewska, *Catal. Today*, 1992, **11**, 597-610.
10. K. Poplawski, J. Lichtenberger, F. J. Keil, K. Schnitzlein and M. D. Amiridis, *Catal. Today*, 2000, **62**, 329-336.
11. J. Lichtenberger and M. D. Amiridis, *J. Catal.*, 2004, **223**, 296-308.
12. A. Khaleel and A. Al-Nayli, *Appl. Catal. B-Environ.*, 2008, **80**, 176-184.
13. W. Tian, X. Y. Fan, H. S. Yang and X. B. Zhang, *J. Hazard. Mater.*, 2010, **177**, 887-891.
14. X. Y. Fan, H. S. Yang, W. Tian, A. M. Nie, T. F. Hou, F. M. Qiu and X. B. Zhang, *Catal. Lett.*, 2011, **141**, 158-162.
15. A. Bellifa, A. Choukchou-Braham, C. Kappenstein and L. Pirault-Roy, *RSC Advances*, 2014, **4**, 22374-22379.
16. S. Alavi, H. Hosseini-Monfared and P. Aleshkevych, *RSC Advances*, 2014, **4**, 48827-48835.
17. Y. Yan, L. Wang and H. P. Zhang, *Chem. Eng. J.*, 2014, **255**, 195-204.
18. W. X. Tang, X. F. Wu, S. D. Li, W. H. Li and Y. F. Chen, *Catal. Commun.*, 2014, **56**, 134-138.
19. B. Q. Jiang, Y. Liu and Z. B. Wu, *J. Hazard. Mater.*, 2009, **162**, 1249-1254.
20. H. C. Wang, H. S. Liang and M. B. Chang, *J. Hazard. Mater.*, 2011, **186**, 1781-1787.
21. H. Einaga and A. Ogata, *J. Hazard. Mater.*, 2009, **164**, 1236-1241.
22. H. Einaga and S. Futamura, *J. Catal.*, 2004, **227**, 304-312.
23. H. S. Liang, H. C. Wang and M. B. Chang, *Ind. Eng. Chem. Res.*, 2011, **50**, 13322-13329.
24. S. Iijima, *Nature*, 1991, **354**, 56-58.
25. R. T. Yang, R. Q. Long, J. Padin, A. Takahashi and T. Takahashi, *Ind. Eng. Chem. Res.*, 1999, **38**, 2726-2731.
26. R. Q. Long and R. T. Yang, *J. Am. Chem. Soc.*, 2001, **123**, 2058-2059.
27. W. Tian, H. S. Yang, X. Y. Fan and X. B. Zhang, *Catal. Commun.*, 2010, **11**, 1185-1188.
28. E. O. Pentsak, E. G. Gordeev and V. P. Ananikov, *ACS Catalysis*, 2014, **4**, 3806-3814.
29. R. Chen, D. D. Jin, H. S. Yang, Z. X. Ma, F. Liu and X. B. Zhang, *Catal. Lett.*, 2013, **143**, 1207-1213.
30. Q. Li, H. S. Yang, A. M. Nie, X. Y. Fan and X. B. Zhang, *Catal. Lett.*, 2011, **141**, 1237-1242.
31. H. Chen, A. Sayari, A. Adnot and F. Larachi, *Appl. Catal. B-Environ.*, 2001, **32**, 195-204.
32. H. Chen, Y. Yan, Y. Shao and H. Zhang, *RSC Advances*, 2014, **4**, 55202-55209.
33. W. X. Tang, W. H. Li, D. Y. Li, G. Liu, X. F. Wu and Y. F. Chen, *Catal. Lett.*, 2014, **144**,

1900-1910.

34. L. Chen, J. H. Li and M. F. Ge, *J. Phys. Chem. C*, 2009, **113**, 21177-21184.
35. M. Kang, E. D. Park, J. M. Kim and J. E. Yie, *Appl. Catal. A-Gen.*, 2007, **327**, 261-269.
36. A. M. Nie, H. S. Yang, Q. Li, X. Y. Fan, F. M. Qiu and X. B. Zhang, *Ind. Eng. Chem. Res.*, 2011, **50**, 9944-9948.
37. J. Carno, M. Ferrandon, E. Bjornbom and S. Jaras, *Appl. Catal. A-Gen.*, 1997, **155**, 265-281.
38. K. Ramesh, L. W. Chen, F. X. Chen, Y. Liu, Z. Wang and Y. F. Han, *Catal. Today*, 2008, **131**, 477-482.
39. B. Dhandapani and S. T. Oyama, *Appl. Catal. B-Environ.*, 1997, **11**, 129-166.
40. H. C. Wang, H. S. Liang and M. B. Chang, *Chemosphere*, 2011, **82**, 1090-1095.
41. W. Li and S. T. Oyama, in *Studies in Surface Science and Catalysis*, eds. R. K. Grasselli, S. T. Oyama, A. M. Gaffney and J. E. Lyons, Elsevier, 1997, vol. 110, pp. 873-882.
42. S. T. Oyama, *Catal. Rev.-Sci. Eng.*, 2000, **42**, 279-322.
43. B. Dhandapani and S. T. Oyama, *Chem. Lett.*, 1995, 413-414.

Figure and Table Captions:

Fig.1. XRD patterns of fresh and 240 h tested MnO_x/CNTs.

Fig.2. SEM images of (a), (b), (c) fresh; and (d), (e), (f) 240 h tested MnO_x/CNTs.

Fig.3. XPS fully scanned spectra of fresh and 240 h tested MnO_x/CNTs.

Fig.4. XPS analysis of fresh and 240 h tested MnO_x/CNTs: (a) fitted Mn $2p_{1/2}$ and Mn $2p_{3/2}$ photoelectron peaks; (b) fitted O 1s photoelectron peaks.

Fig.5. H_2-TPR profiles of fresh and 240 h tested MnO_x/CNTs.

Fig.6. Temperature dependent of CB catalytic oxidation over MnO_x/CNTs with and without O_3.

Fig.7. CB complete conversion under conditions of 50 ppm CB and O_3. For comparison, the oxidation of CB by 513 ppm O_3 only was also presented.

Fig.8. Dependence of r on O_3 concentration over MnO_x/CNTs at 120 °C (the inset is the plot of apparent k) and Arrhenius plot of CB catalytic oxidation over MnO_x/CNTs with the assistance of O_3.

Table.1. Surface element compositions of the fresh and 240 h tested MnO_x/CNTs Calculated from the XPS results.

Samples	Mn (at.%)	O (at.%)	O_{latt} (at.%)	O_{ads} (at.%)	O_{sur} (at.%)	Mn^{4+}/Mn^{3+}
fresh MnO_x/CNTs	1.64	8.16	2.75	4.17	1.24	4.03
used MnO_x/CNTs	1.54	9.65	1.85	5.81	1.99	1.97

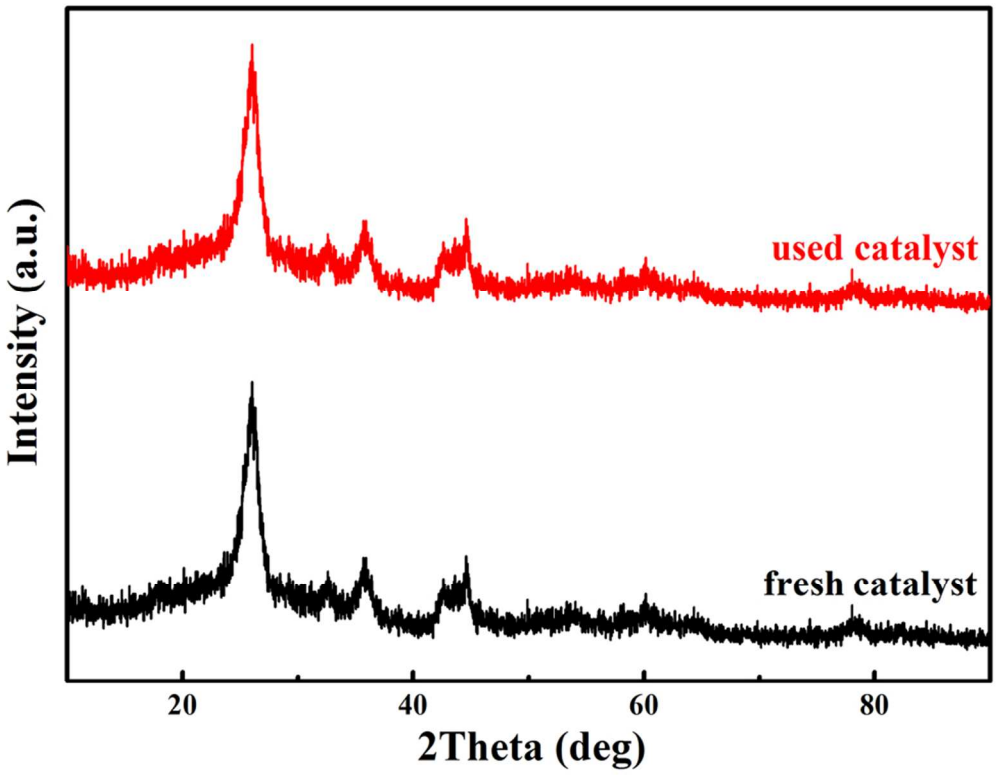

Fig. -1 XRD patterns of fresh and 240 h tested MnOx/CNTs.
82x64mm (300 x 300 DPI)

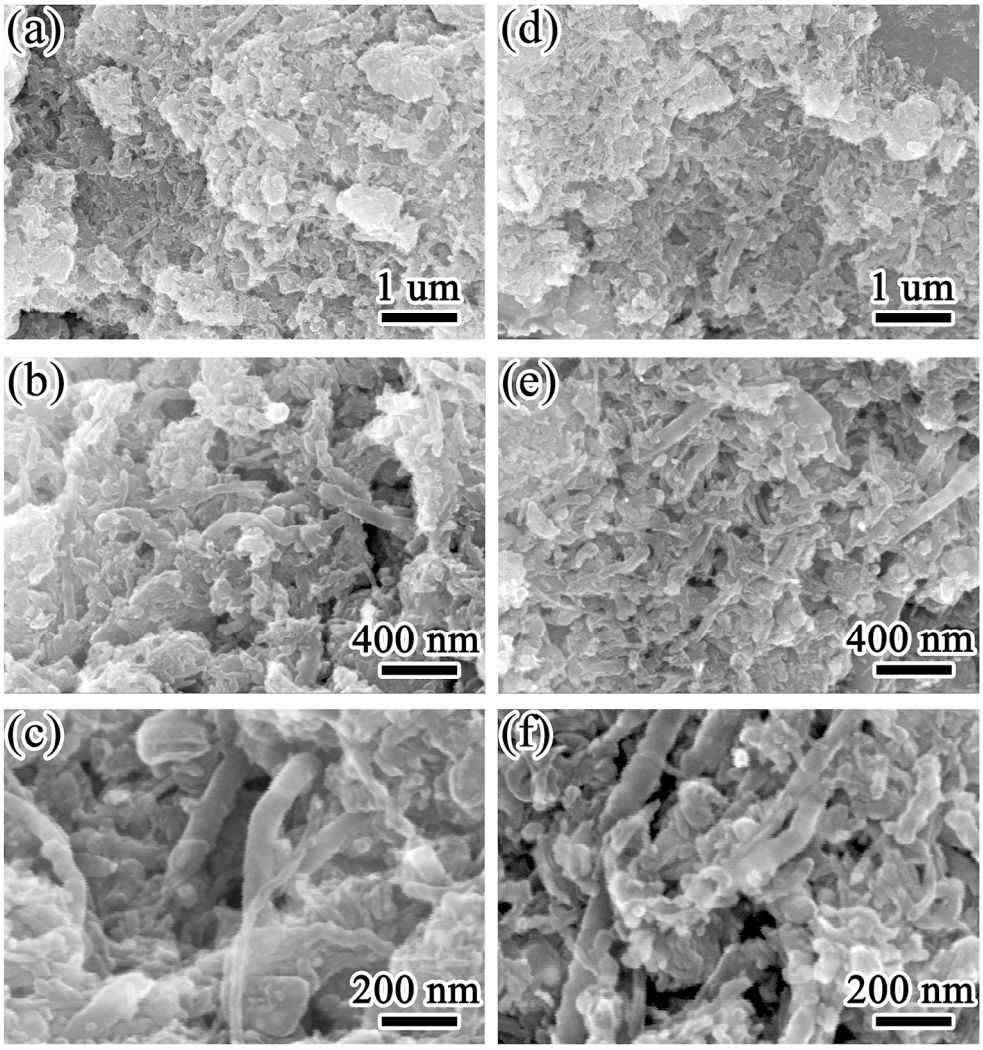

SEM images of (a), (b), (c) fresh; and (d), (e), (f) 240 h tested MnOx/CNTs.
171x181mm (300 x 300 DPI)

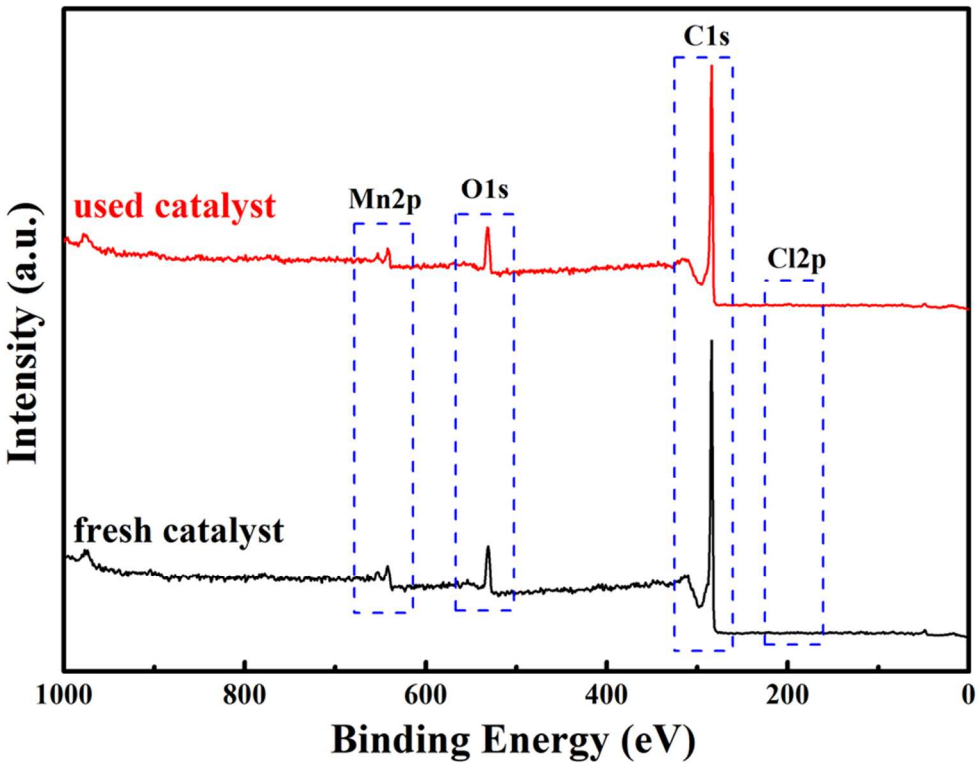

XPS fully scanned spectra of fresh and 240 h tested MnOx/CNTs.
82x64mm (300 x 300 DPI)

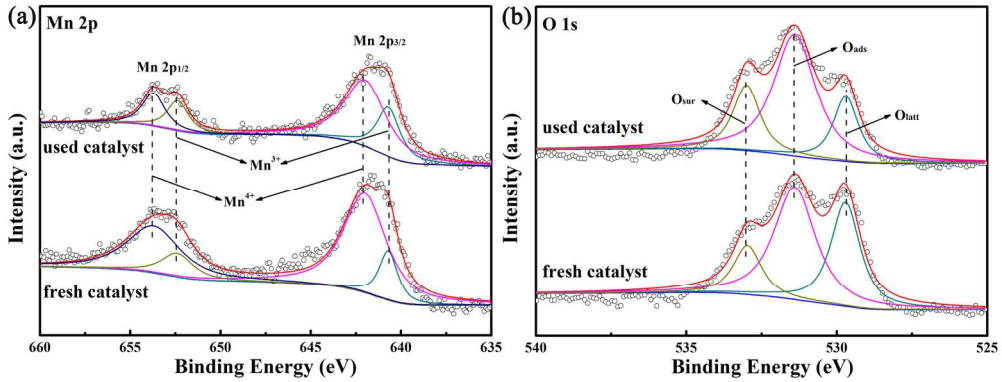

XPS analysis of fresh and 240 h tested MnOx/CNTs: (a) fitted Mn 2p1/2 and Mn 2p3/2 photoelectron peaks; (b) fitted O 1s photoelectron peaks.
171x65mm (300 x 300 DPI)

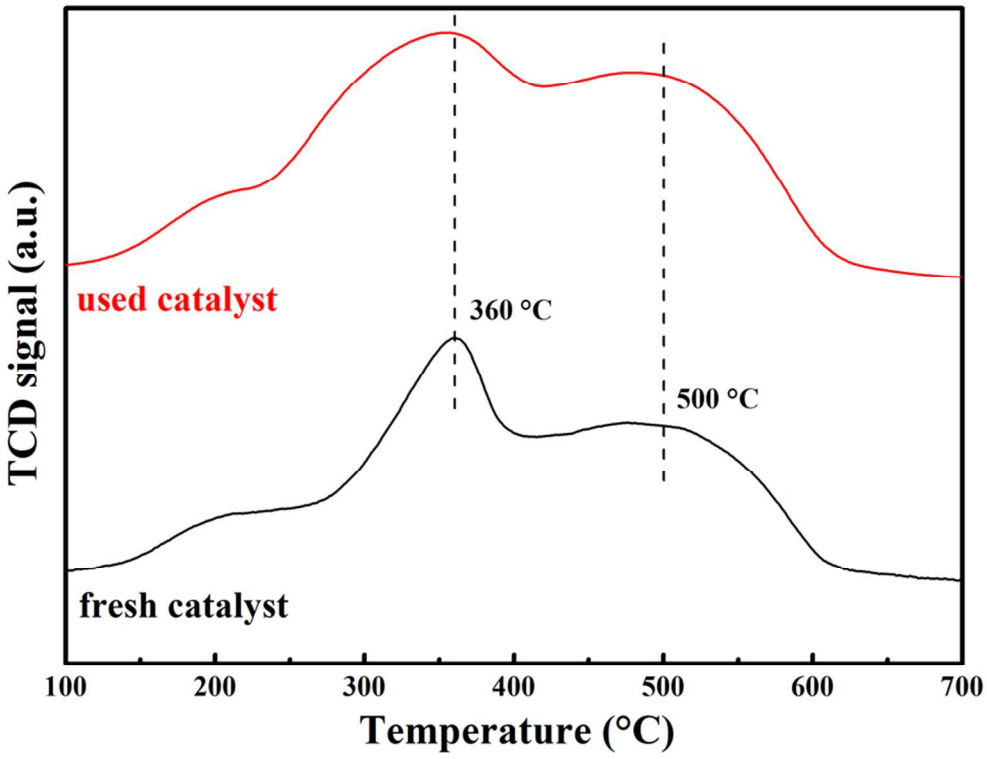

H2-TPR profiles of fresh and 240 h tested MnOx/CNTs.
82x64mm (300 x 300 DPI)

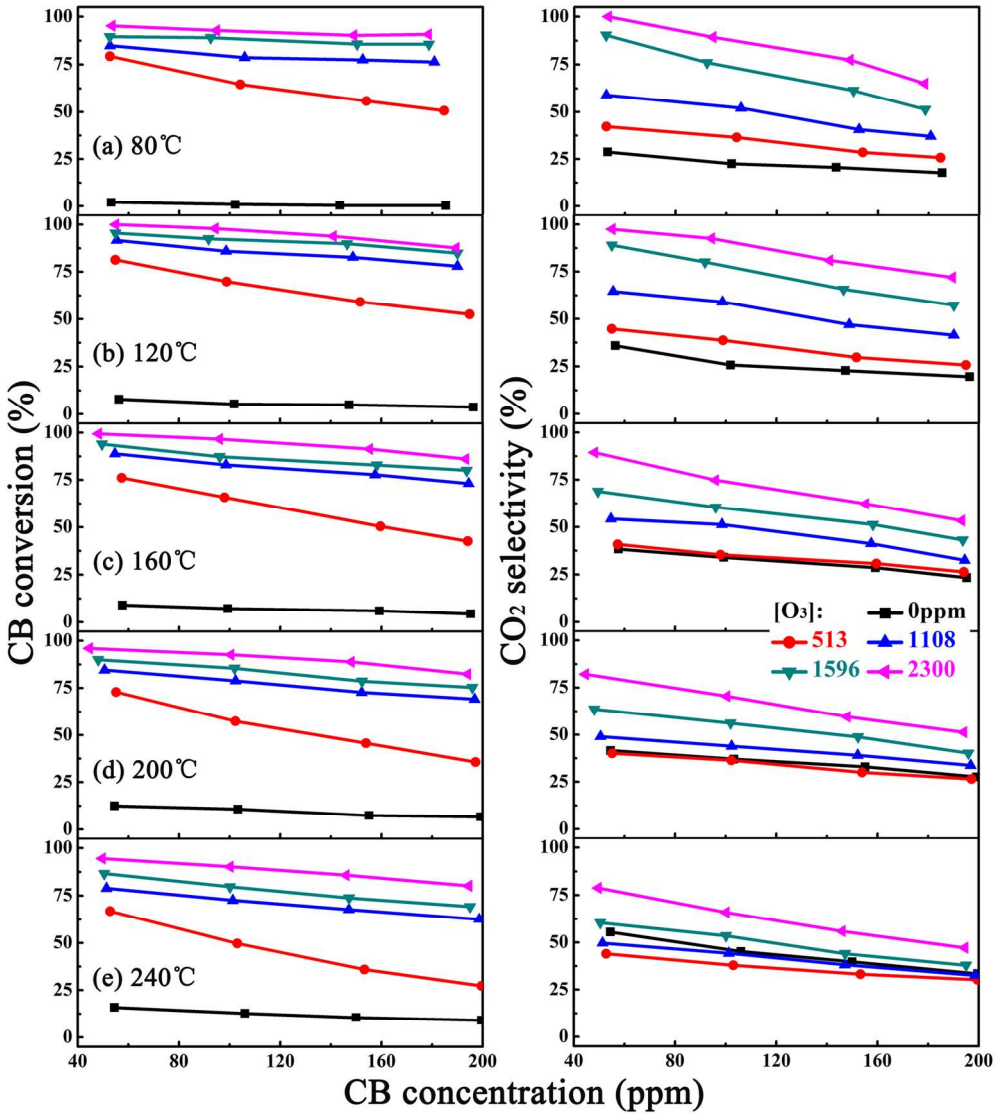

Temperature dependent of CB catalytic oxidation over MnOx/CNTs with and without O3.
171x192mm (300 x 300 DPI)

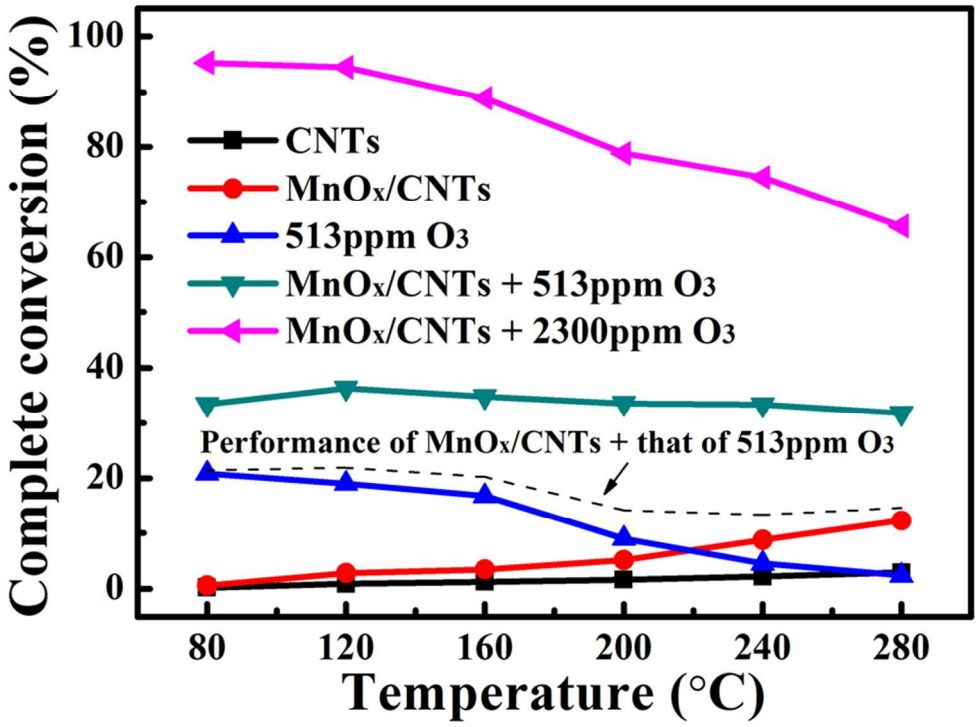

CB complete conversion under conditions of 50 ppm CB and O3. For comparison, the oxidation of CB by 513 ppm O3 only was also presented.
82x61mm (300 x 300 DPI)

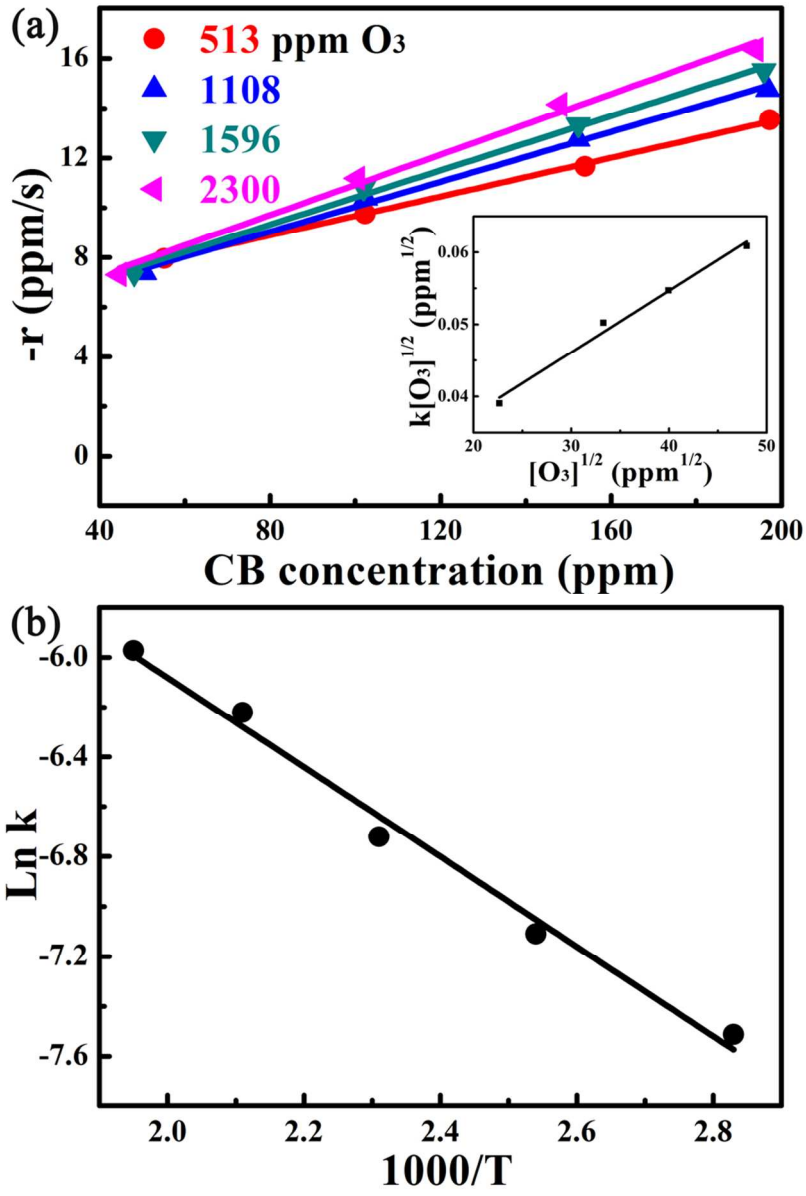

Dependence of r on O3 concentration over MnOx/CNTs at 120 °C (the inset is the plot of apparent k) and Arrhenius plot of CB catalytic oxidation over MnOx/CNTs with the assistance of O3.
82x121mm (300 x 300 DPI)